ISSN: 2414-1895 DOI: 10.6919/ICJE.202307_9(7).0023

Mechanical Properties of Phenine Nanotube Bundles

Yanjun Liu

Faculty of Civil Engineering and Mechanics, Jiangsu University, Zhenjiang, Jiangsu 210013, China

*liuyanjun01212@163.com

Abstract

Since the discovery of carbon nanotubes, they have attracted great attention from many fields because of their unique structure and excellent mechanical, electrical and thermal properties. However, perfect carbon nanotubes have poor load transfer ability. In addition, different defect configurations in the experimentally produced carbon nanotubes, which will change the electronic properties of the system. Therefore, installing periodic defects in carbon nanotubes can well manipulate its electronic properties and provide a new idea for increasing its load transfer ability. Phenine nanotubes have good intrinsic semiconductor bandgap and special topological structure, they have been successfully synthesized in recent experiments and are expected to become a potential alternative to carbon nanotubes in functional devices. In this paper, molecular dynamics simulation was used to study the mechanical properties of phenine nanotubes, the mechanical response of phenine nanotube bundles under different loading modes were calculated.

Keywords

Molecular Dynamics; Phenine Nanotubes; Mechanical Property.

1. Introduction

As a novel one-dimensional carbon nanomaterial, phenine nanotubes have high potential applications in semiconductor devices due to their intrinsic semiconductor energy gap and special topological structure [1-4]. This structure, with extremely strong sp2 carbon-carbon bonds and low density since it is allotrope of carbon, has special structural and mechanical properties, and is expected to be used to construct lightweight and high-strength functional materials. Compared with the perfect carbon nanotubes and other materials that have been widely and deeply studied [5-13], the academic community's understanding of the properties of phenine nanotubes is not enough, especially its basic physical and mechanical properties need to be systematically explored, and it also lays a theoretical foundation for the design of high-performance materials based on phenine nanotubes.

2. Methods and Experimental Detail

All simulations were carried out using the large-scale atomic/molecular massively parallel simulator (LAMMPS) package [14]. The OVITO package is used for visualization. To describe interatomic interactions, the AIREBO potential [15] was adopted, which has been successfully applied to study the structural and mechanical properties of carbon nanomaterials. The cutoff distance is modified to 2 Å to avoid nonphysical description of mechanical properties by the original AIREBO potential [16-18]. Geometry optimization was first conducted using the conjugate gradient method with periodic boundary conditions; the system was then relaxed in the NVT ensemble with a time step of 1 fs to reach an equilibrium state. For the investigation of mechanical properties, the bundle was uniformly stretched/shear along its axial/radial direction with a strain rate of 0.1/ps until failure in the NVT

ISSN: 2414-1895 DOI: 10.6919/ICJE.202307_9(7).0023

ensemble at 1 K. The distance between the two adjacent tube cores is set at 2.5R, where R is the radius of phenine nanotubes, so as to avoid too close a distance that would attract phenine nanotubes together due to van der Waals action in the relaxation process.

3. Results and Discussion

3.1 Mechanical Properties of Phenine Nanotube Bundles under Tensile Load

In this section, the mechanical properties of the bundle structures of two phenine nanotubes in parallel arrangement and four, nine and sixteen phenine nanotubes in square arrangement under axial tensile and radial shear loads are mainly explored through molecular dynamics simulation. The armchair phenine nanotube with diameter of 16.50 Å, 24.75 Å, 33.00 Å, 41.25 Å and 61.88 Å with aspect ratio of 7:1 was considered. The zigzag phenine nanotube with aspect ratio of 7:1 and diameter of 11.91 Å, 23.82 Å, 33.34 Å, 42.87 Å and 61.92 Å, their cross-sectional configuration is shown below, see Figure 1.

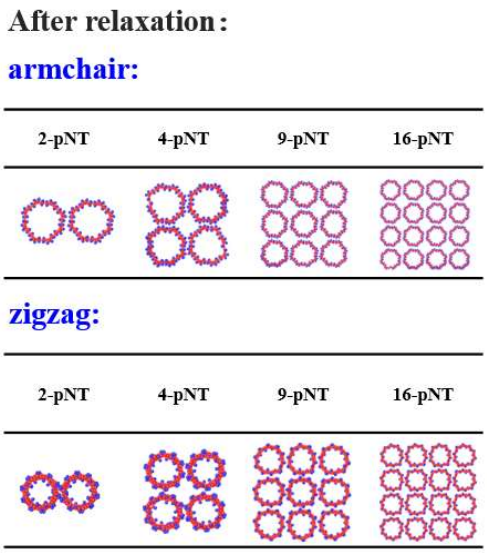

Figure 1. A cross section view of the tube bundles structure of the phenine nanotube in square arrangement after relaxation

As shown in Figure 2, the stress increases linearly with the increase of strain. When a certain strain is reached, a nonlinear response of stress occurs, and the stress increases slowly. Then, with the increase of strain, the stress decreases to 0. The mechanical properties of armchair phenine nanotubes and zigzag phenine nanotubes are different, and the former is slightly better than the latter. This is because when axial tensile loads are applied to armchair and serrated phenine nanotube bundle structures, in armchair structures, the load is mainly borne by continuous C-C chains distributed along the axial direction. However, in the zigzag structure, the load is mainly carried by the axial distribution and discontinuous carbon-carbon bond. Obviously, the load bearing capacity of continuous carbon-carbon chain is higher than that of carbon-carbon bond. Under the same length-diameter ratio, the mechanical properties of tube bundle structure first decrease and then converge with the increase of diameter.

Figure 3 shows some fracture snapshots of phenine nanotube bundle structures arranged side-by-side with aspect ratio of 7:1 under tensile load. The fracture mode of its tube bundle structure is similar to the fracture failure process of single phenine nanotubes. When the critical fracture strain is reached, the carbon-carbon bond parallel to the tube axis firstly breaks, and then with the increase of strain, The initial crack gradually expanded (at this time, the carbon-carbon bond was still broken along the tube axis) until the phenine nanotubes were completely broken. It is observed that the fracture surface

ISSN: 2414-1895 DOI: 10.6919/ICJE.202307_9(7).0023

of the armchair bundles structure is not very smooth, while the fracture surface of the sawtooth bundle structure is relatively smooth. In addition, it can be observed from the stress-strain curves of all the simulated serrated bundle structures.

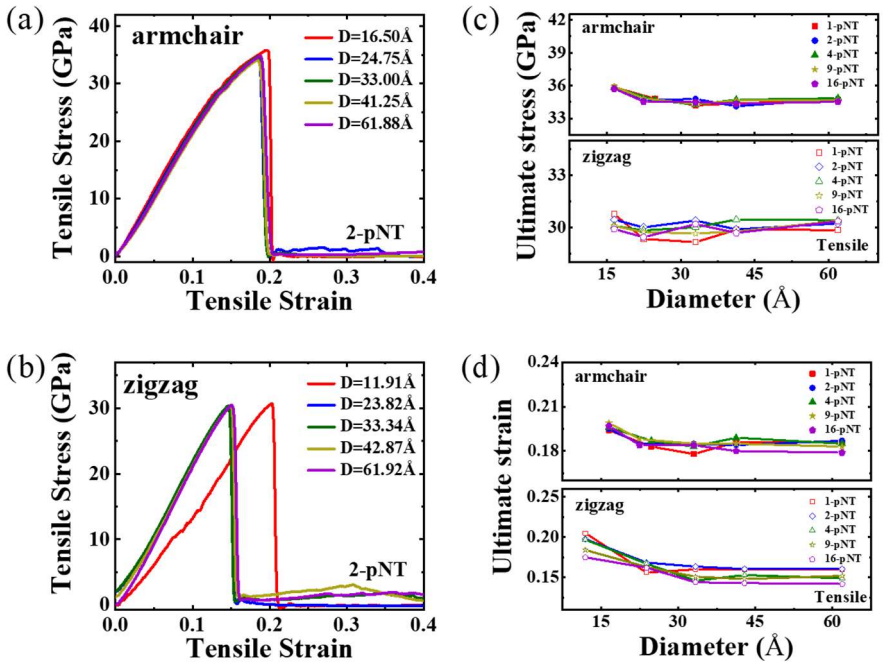

Figure 2. Stress-strain relationship of phenine nanotube bundles with length-diameter ratio of 7:1 under tensile load

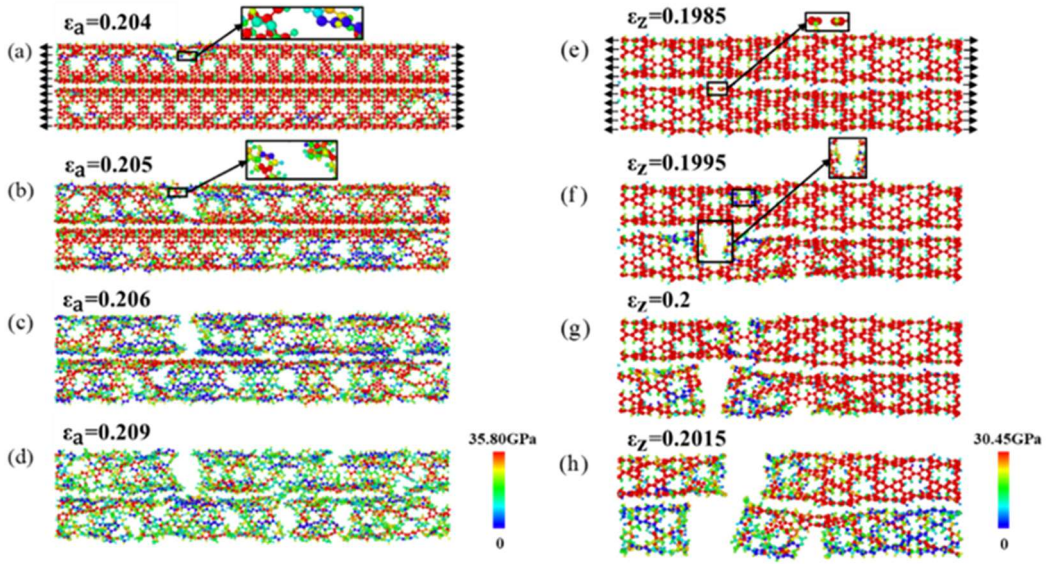

Figure 3. Fracture of parallel-arranged armchair (a-d in left panel) and zigzag (e-h in right panel) phenine nanotube bundles under tensile. The initial location, nucleation, and subsequent propagation of the crack are marked in snapshots in insets of (a-d) and (e-h). ϵa denotes strain along armchair direction and ϵz denotes strain along zigzag direction

3.2 Mechanical Properties of Phenine Nanotube Bundles under Tensile Load

Figure 4 shows the stress-strain relationship diagram. It can be clearly seen from Figure 4 (a) and (b) that the mechanical response of armchair type and zigzag type phenine nanotubes under shear load is significantly different. Firstly, the ultimate stress of armchair phenine nanotube bundles under shear

ISSN: 2414-1895 DOI: 10.6919/ICJE.202307_9(7).0023

load is higher than that of the zigzag type, and the diameter makes the mechanical properties of armchair tube bundles decrease overall, but the range is small. Secondly, compared with the mechanical response of armchair bundle under shear load, the stress-strain curve of zigzag bundle is only half of the former, and the diameter of zigzag bundle structure has a greater impact on the mechanical response, the ultimate stress and ultimate strain increase monotonically with the increase of the diameter. The stress-strain curve is linear under small strain, and becomes nonlinear with the increase of strain. The ultimate stress and ultimate strain of the above bundle structure have the same variation trend.

Figure 5 shows the dynamic structural change process of parallel double-rooted nanotubes with an aspect ratio of 7:1 under shear load. It can be seen from the analysis that the fracture failure process under shear load is the same as that under the tensile load mentioned above. In the armchair tube bundle, the continuous carbon-carbon chain is still under shear load. However, the shear load of the serrated nanotube bundle is mainly carried out by the carbon-carbon bond distributed along the axial direction, so the mechanical properties of the serrated nanotube bundle are significantly lower than that of the armchair bundle. It can be seen from Figure 5 that the fracture surface of armchair bundle structure is not very smooth, while that of serrated bundle structure is relatively smooth. The failure of tube bundles of phenine nanotubes still follows the above fracture form, that is, when the critical fracture strain reaches 63.6%, bond fracture begins to occur on the tube, and with the increase of strain, cracks expand rapidly until the structure breaks and fails. Combined with the dynamic behavior of other tube bundle structure fracture failure, it can be observed that the initial failure is always in the corner position of the nanotubes, because the nanotubes in the corner position is more prone to stress concentration. And although the overall carrying capacity of the model structure is improved with the increase of the number of phenine nanotubes in the model, due to the corresponding increase of the effective area of its section, each nanotube equally apportioned to the bundle structure shows no significant change in its mechanical properties.

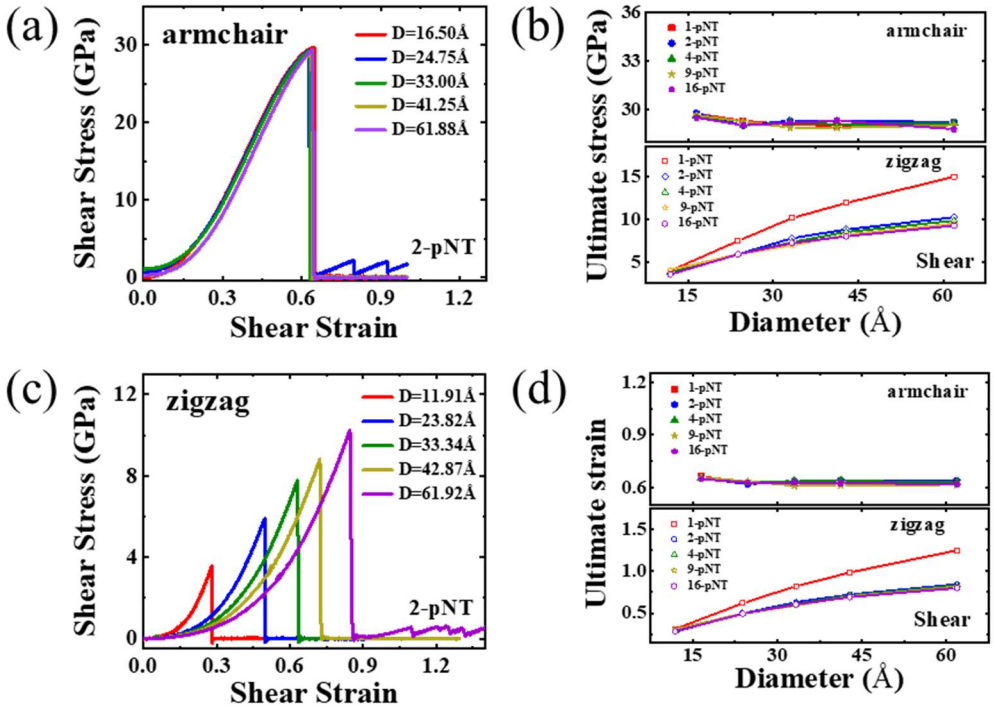

Figure 4. Stress-strain relationship of phenine nanotube bundles with length-diameter ratio of 7:1 under shear load

ISSN: 2414-1895 DOI: 10.6919/ICJE.202307_9(7).0023

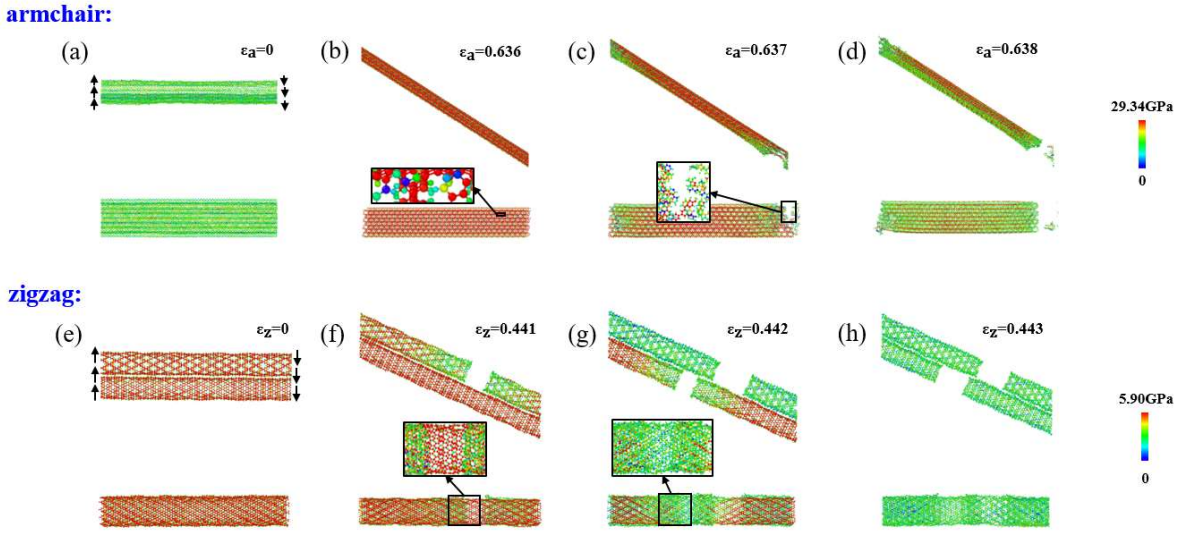

Figure 5. Fracture of parallel-arranged phenine nanotube bundles under shear load. (a-d) and (e-h) respectively correspond to the front view and the corresponding side view of the structure in the simulation process, the initial location, nucleation, and subsequent propagation of the crack are marked in snapshots in insets. ϵa denotes shear strain along armchair direction, ϵz denotes shear strain along armchair direction

4. Conclusion

In summary, this study investigated the molecular dynamics simulation of loading mode, chirality and diameter on the phenine nanotube bundle model. This study shows that the mechanical properties of chiral nanotube bundles are significantly different under tensile and shear loads due to the different loading modes in the bundle. The mechanical properties of armchair nanotube bundles are better than those of sawtooth nanotube bundles. This is attributed to the fact that in the armchair nanotube, the continuous carbon-carbon chains along the axial direction mainly bear the external load, while in the serrated nanotube, the load is mainly borne by the carbon-carbon bonds distributed along the tube axis. And the increase of the number of tube bundles will not improve its mechanical properties, mainly because with the increase of the number of tubes in the model, the overall bearing capacity of the model structure is improved, but because the effective area of the section is also increased, so the average allocation to each tube bundle structure of the nanotube, its mechanical properties did not change greatly. These results have guiding significance for the preparation and design of lightweight high-strength nanofiber structures.

Acknowledgments

Natural Science Foundation.

References

[1] Sun Z, Ikemoto K, Fukunaga T M, et al. Finite phenine nanotubes with periodic vacancy defects. Science, 2019, 363(6423): 151-155.

[2] Stasyuk A J, Stasyuk O A, Sola M, et al. Photoinduced electron transfer in nanotube supersetC(70) inclusion complexes: phenine vs. nanographene nanotubes. Chemical Communications 2020, 56(83): 12624-12627.

[3] Stasyuk O A, Stasyuk A J, Sola M, et al. How Do Defects in Carbon Nanostructures Regulate the Photoinduced Electron Transfer Processes? The Case of Phenine Nanotubes. Chemphyschem, 2021, 22 (12): 1178-1186.

[4] Walsh J C, Bodwell G J. The phenine concept delivers a nitrogen-doped nanotube and evokes infinite possibilities. Commun Chem, 2020, 3(1): 94.

ISSN: 2414-1895 DOI: 10.6919/ICJE.202307_9(7).0023

[5] Yi B, Ramakrishnan R, Foley H C, et al. Catalytic polymerization and facile grafting of poly(furfuryl alcohol) to single-wall carbon nanotube: preparation of nanocomposite carbon. Journal of the American Chemical Society, 2006, 128(34): 11307-13.

[6] Vigolo B, Pénicaud A, Coulon C, et al. Macroscopic fibers and ribbons of oriented carbon nanotubes. Science, 2000, 290(5495): 1331-1334.

[7] Iijima T, Oshima H, Hayashi Y, et al. In-situ observation of carbon nanotube fiber spinning from vertically aligned carbon nanotube forest. Diamond and Related Materials, 2012, 24: 158-160.

[8] Mcdonough M A, Schofield C J. New Structural Insights into the Inhibition of Serine Proteases by Cyclic Peptides from Bacteria. Chemistry & Biology, 2003, 10(10): 898-900.

[9] Gao J, Itkis M E, Yu A, et al. Continuous spinning of a single-walled carbon nanotube-nylon composite fiber. Journal of the American Chemical Society, 2005, 127(11): 3847-3854.

[10] Jee M H, Choi J U, Park S H, et al. Influences of tensile drawing on structures, mechanical, and electrical properties of wet-spun multi-walled carbon nanotube composite fiber. Macromolecular Research, 2012, 20(6): 650-657.

[11] Liu C, Cheng H M, Cong H, et al. Synthesis of macroscopically long ropes of well-aligned single-walled carbon nanotubes. Advanced Materials, 2000, 12(16): 1190-1192.

[12] Iijima S. Helical microtubules of graphitic carbon. Nature, 1991, 354(6348): 56-58.

[13] Liu C, Fan Y Y, Liu M, et al. Hydrogen Storage in Single-Walled Carbon Nanotubes at Room Temperature [J]. Science, 1999, 286(5442): 1127-1129.

[14] Plimpton S. Fast parallel algorithms for short-range molecular dynamics [J]. Journal Of Computational Physics, 1995, 117(1): 1-19.

[15] Stuart S J, Tutein A B, Harrison J a J J O C P. A reactive potential for hydrocarbons with intermolecular interactions [J]. The Journal of Physical Chemistry, 2000, 112: 6472-6486.

[16] Zhan H, Zhang G, Tan V B C, et al. From brittle to ductile: a structure dependent ductility of diamond nanothread [J]. Nanoscale, 2016, 8(21): 11177-11184.

[17] Zhao H, K. M, Aluru N R. Size and chirality dependent elastic properties of graphene nanoribbons under uniaxial tension [J]. Nano Letters, 2009, 9(8): 3012-5.

[18] Carpenter C, Maroudas D, Ramasubramaniam A. Mechanical properties of irradiated single-layer graphene [J]. Applied Physics Letters, 2013, 103: 013102.